DNA–Cholesterol Barges as Programmable Membrane-Exploring Agents

Alexander Johnson-Buck,[†] Shuoxing Jiang,[‡,§] Hao Yan,[‡,§] and Nils G. Walter[†,*]

[†]Single Molecule Analysis Group, Department of Chemistry, University of Michigan, 930 North University Avenue, Ann Arbor, Michigan 48109-1055, United States, [‡]The Biodesign Institute, Arizona State University, Tempe, Arizona 85287, United States, and [§]Department of Chemistry and Biochemistry, Arizona State University, Tempe, Arizona 85287, United States

ABSTRACT DNA nanotechnology enables the precise construction of nanoscale devices that mimic aspects of natural biomolecular systems yet exhibit robustly programmable behavior. While many important biological processes involve dynamic interactions between components associated with phospholipid membranes, little progress has been made toward creating synthetic mimics of such interfacial systems. We report the assembly and characterization of cholesterol-labeled DNA origami "barges" capable of reversible association with and lateral diffusion on supported lipid bilayers. Using single-particle fluorescence microscopy, we show that these DNA barges rapidly and stably embed in lipid bilayers and exhibit Brownian diffusion in a manner dependent on both cholesterol labeling and bilayer composition. Tracking of individual barges rapidly generates super-resolution maps of the contiguous regions of a membrane. Addition of appropriate command oligonucleotides enables membrane-associated barges to reversibly exchange fluorescent cargo with bulk solution, dissociate from the membrane, or form oligomers within the membrane, opening up new possibilities for programmable membrane-bound molecular devices.

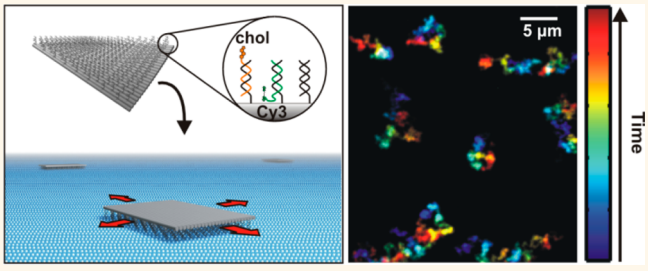

KEYWORDS: DNA origami · DNA nanotechnology · lipid bilayer · diffusion · single-particle tracking

Membrane-bound protein complexes carry out many vital functions in the cell, including critical roles in signal transduction, transport, energy metabolism, and cell adhesion.[1−13] Many of these functions involve highly specific, yet dynamic interactions that require lateral diffusibility within the membrane as well as accessibility to the adjacent extracellular matrix and/or the cytoplasm. For instance, the biological activity of many receptors depends on their ligand-triggered aggregation or dimerization within the membrane,[1,8,11,12] and a single activated cell-surface receptor may amplify its signal by serially activating multiple copies of a downstream membrane-bound G-protein.[5,7,13] The capacity to construct programmable synthetic counterparts to these dynamic interfacial systems will enable new approaches in biosensing and synthetic biology.

Recently, significant progress has been made toward mimicking some features of membrane proteins using DNA nanotechnology. For instance, two groups have recently constructed synthetic membrane-spanning nanopores using the DNA origami technique.[14−16] In these studies, ion channels are designed to associate with lipid bilayers *via* site-specific labeling with cholesterol, ethyl phosphorothioate, or tetraphenylporphyrin moieties, causing detectable changes in conductance across the bilayer by localized disruption. In another report, cholesterol-modified DNA origami rods were shown to associate with giant unilamellar vesicles, partitioning between lipid phases in a metal ion-dependent manner.[17] While lateral diffusion of some of these membrane-associated DNA nanostructures has been observed,[16,17] this property has not yet been characterized at the single-particle level, nor has it been exploited to engineer programmable interactions between membrane-embedded nanostructures. Furthermore, nonspecific binding of the DNA structures to lipid bilayers has emerged as a possible impediment to highly specific

* Address correspondence to nwalter@umich.edu.

Received for review January 7, 2014 and accepted May 15, 2014.

Published online May 15, 2014
10.1021/nn500108k

and programmable behavior.[14] To further develop the potential applications of diffusible membrane-anchored DNA devices, it is important to determine what factors influence their interactions with lipid bilayers, their diffusive behavior within the bilayer, and their capacity to undergo rationally programmable interactions with membranes and other binding partners while embedded within a membrane.

In this work, we introduce rectangular cholesterol-labeled DNA origami "barges" (so named to contrast them with previously described DNA "rafts"[18]) as a platform for rationally engineering molecular behaviors within phospholipid membranes. Using single-particle fluorescence microscopy, we show that DNA barges become anchored in a supported lipid bilayer within a few minutes and remain stably bound, undergoing normal two-dimensional Brownian motion with diffusion coefficients similar to typical lipid-linked membrane proteins. We find that the cholesterol labels, composition of the membrane, buffer conditions, and interaction surface of the DNA tile all influence the ability of origami to associate with and diffuse laterally within a supported lipid bilayer. We further show that DNA barges can be used as super-resolution probes of membrane structure, rapidly mapping out contiguous regions of membrane with high spatial accuracy. Finally, we demonstrate the ability of membrane-embedded DNA barges to execute programmable behaviors such as loading and unloading of cargo, detachment from the membrane, and oligomerization with other DNA barges, opening up new possibilities for engineering sophisticated membrane-embedded molecular systems.

RESULTS AND DISCUSSION

For the design of our DNA barges, we chose a classic rectangular (~60 × 90 × 2 nm) origami scaffold[19] based on its reliable assembly and planar topology, which we reasoned would permit stable and well-defined interactions with a lipid bilayer. The overall dimensions of the scaffold are slightly larger than those of large membrane-associated protein complexes such as the photosystems and light-harvesting complexes of plants and cyanobacteria (10−70 nm in diameter).[20−22] We extended 187 of the single-stranded DNA (ssDNA) staples with 20-nucleotide probe sequences as previously described[23] to permit the specific attachment of complementary cholesterol-labeled ssDNA Anchor (*A*) strands to one face of the origami *via* hybridization, creating a hydrophobic surface by which the barge can interact with lipid bilayers (Figure 1a). The ssDNA overhangs alternatively permit the attachment of fluorescently labeled Cargo (*C*) strands that have the same sequence as *A* but carry an 8-nucleotide single-stranded toehold extension (Figure 1a) for use in single-particle tracking and studies of programmable barge behaviors. In some experiments, a third unlabeled Passenger DNA strand (*P*) with the same

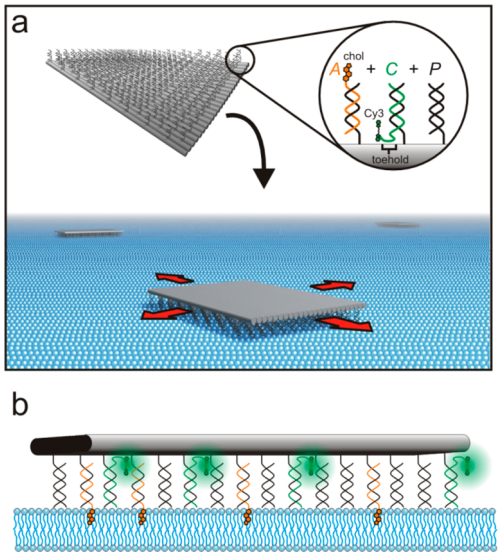

Figure 1. Design of DNA−cholesterol barges. (a) A rectangular DNA origami bearing 187 identical 20-nucleotide ssDNA overhangs on one face is coated with cholesterol-conjugated anchor strands (*A*) and Cy3-labeled Cargo strands (*C*) by hybridization. The cholesterol label permits stable association with, and lateral diffusion within, supported lipid bilayers. (b) Expected mode of interaction between a DNA barge and a supported lipid bilayer. For clarity, only a single row of dsDNA extensions is shown.

sequence as *A* (lacking the toehold) was used to act as a rigid spacer between the origami tile and the lipid bilayer without introducing additional cholesterol or fluorescent labels. The same capture probe sequence was used to attach *A*, *C*, and *P* to the DNA origami; while this results in random deposition of the oligonucleotides on the origami surface, it allowed us to freely vary the average number of cholesterol and Cy3 labels per tile using the same origami platform design. Importantly, fluorescence assays using agarose gel electrophoresis indicated that *C* and *P* bind to the origami tile with similar kinetics, but that *A* binds 6−9 times more slowly (Figure S1, Supporting Information). The latter difference may result from the formation of micelles by the cholesterol-conjugated *A* strand in solution, as determined by dynamic light scattering (DLS) and native polyacrylamide gel electrophoresis (PAGE) (Figure S2, Supporting Information); such micelles are expected to diffuse more slowly, reducing the rate of encounter with overhangs on the DNA origami tile. Atomic force microscopy reveals that the origami fold into the desired rectangular shape and retain this shape upon addition of *A* (Figure S1, Supporting Information). The expected mode of barge anchoring in lipid bilayers is depicted in Figure 1b.

First, we investigated the tendency of cholesterol-labeled DNA barges to aggregate in aqueous solution. Agarose gel electrophoresis showed that the DNA barges form large aggregates when one of their faces is completely coated with *A* (Figure S1, Supporting Information). However, replacing ≥50% of *A* with *P* and/or *C* during assembly suffices to avoid severe

aggregation. We conclude that coating the DNA–cholesterol barges with a significant fraction of noncholesterol-labeled *P* or *C* results in a discontinuous hydrophobic surface that is less prone to aggregation. On the basis of these findings, DNA barges were prepared using a 1:1:2 mixture of *A*:*C*:*P* for the following experiments, unless otherwise noted.

To characterize the interactions between DNA barges and lipid membranes, barges assembled with *A*, *C*, and *P* were incubated in the presence of a supported lipid bilayer prepared from a 12.5:1 mixture of 1,2-dioleoyl-*sn*-glycero-3-phosphocholine (DOPC) and 1,2-dioleoyl-*sn*-glycero-3-phosphoethanolamine-*N*-[methoxy(poly(ethylene glycol))-550] (DOPE-mPEG) on a quartz microscope slide and imaged by total internal reflection fluorescence (TIRF) microscopy. Barges populate the bilayer within minutes (Figure S3, Movie S1, Supporting Information) and undergo lateral diffusion at the surface of the microscope slide (Figure 2a), remaining bound to the bilayer at a nearly constant density for at least several hours at room temperature (Figure S4, Supporting Information). When the cholesterol-labeled *A* was replaced with *P* (lacking the cholesterol label), the extent of DNA barge binding to the DOPC/DOPE-mPEG bilayer decreased by approximately 50-fold (Figures 2b and S3, Supporting Information), demonstrating that binding to the bilayer is cholesterol-dependent. Interestingly, a small number of barges lacking cholesterol associate with the bilayer and exhibit diffusive behavior similar to cholesterol-modified barges (Figure S5, Supporting Information). Furthermore, when the membrane is constructed from only DOPC (omitting DOPE-mPEG), nonspecific binding in the absence of cholesterol increases ~70-fold (Figure 2b) and results primarily in nondiffusing barges (Figure S6, Supporting Information). This is consistent with prior observations that DNA binds to zwitterionic lipid membranes in the presence of metal cations.[24] Accordingly, when the standard TA-Mg^{2+} buffer (40 mM Tris base, 20 mM acetic acid, 12.5 mM $Mg(CH_3COO)_2$) is replaced with magnesium-free PBS buffer, the extent of nonspecific binding of DNA barges to DOPC-only bilayers is again only 1–2% of cholesterol-mediated binding (Figure S6, Supporting Information), and cholesterol-labeled barges diffuse freely within the bilayer (Figure 3). Importantly, the immobility of barges on DOPC-only bilayers cannot be attributed to a lack of membrane fluidity, which fluorescence recovery after photobleaching (FRAP) experiments suggest is similar to that for DOPC/DOPE-mPEG bilayers (Figure S3c, Supporting Information). Taken together, these results suggest that, while cholesterol anchors are required to obtain a high yield of freely diffusing barges within the membrane, stable association does not strictly depend upon cholesterol, but may also occur *via* other binding modes such as cation-bridged interactions between the origami tile and the phosphatidyl head groups of DOPC. The mPEG-550 modification appears to mitigate these

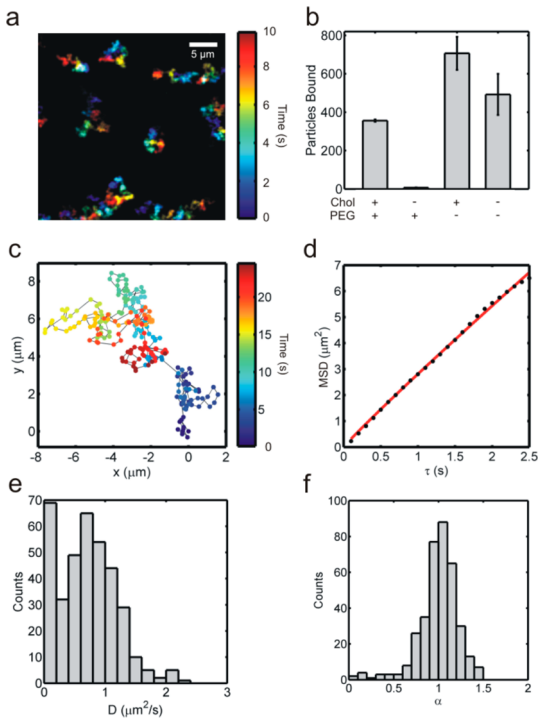

Figure 2. Binding and lateral diffusion of single DNA barges within supported lipid bilayers. (a) Time-lapse image of several DNA barges (assembled with a 1:1:2 mixture of *A*:*C*:*P* oligos) within a DOPC/DOPE-mPEG supported lipid bilayer. Each frame of the raw movie is shown in a different color. (b) Number of barges visible per 50 × 100 μm^2 area after binding reached completion as a function of cholesterol labeling and bilayer composition (DOPC/DOPE-mPEG or DOPC only). Error bars represent one standard deviation from at least 5 measurements on separate fields of view. (c) Trajectory of a single DNA barge within a supported lipid bilayer. (d) Time-averaged mean-square displacement (MSD) plot of the trajectory shown in (c). The red line represents the best-fit line with the anomalous diffusion model MSD = $4D\tau^{\alpha}$. (e) Diffusion coefficients of 365 DNA barges determined by single-particle tracking and MSD analysis ($\langle D \rangle$ = 0.71 μm^2/s). (f) Time exponents derived from MSD analysis of 365 DNA barges ($\langle \alpha \rangle$ = 1.001).

nonspecific interactions, in keeping with its common role as a surface passivating agent[25,26] while still permitting the specific association of origami *via* the cholesteryl anchors (Figure S3d, Supporting Information). Consistent with these observations, cholesterol-labeled DNA barges in either TA-Mg^{2+} or PBS buffer also bind directly to bare (and thus negatively charged) quartz slides, presumably due to nonspecific cation-bridged interactions, and consequently do not undergo lateral diffusion (Figure S6, Supporting Information).

To characterize the motion of cholesterol-labeled DNA barges in DOPC bilayers, we tracked the diffusion of 365 DNA barges (*A*:*C*:*P* = 1:1:2) in several fields of view over time, resulting in position-*versus*-time trajectories of individual barges (Figure 2c). Time-averaged mean-squared displacement (MSD) plots generated from these trajectories typically show a nearly linear increase over time (Figure 2d). Fitting the individual time-averaged MSD plots with the

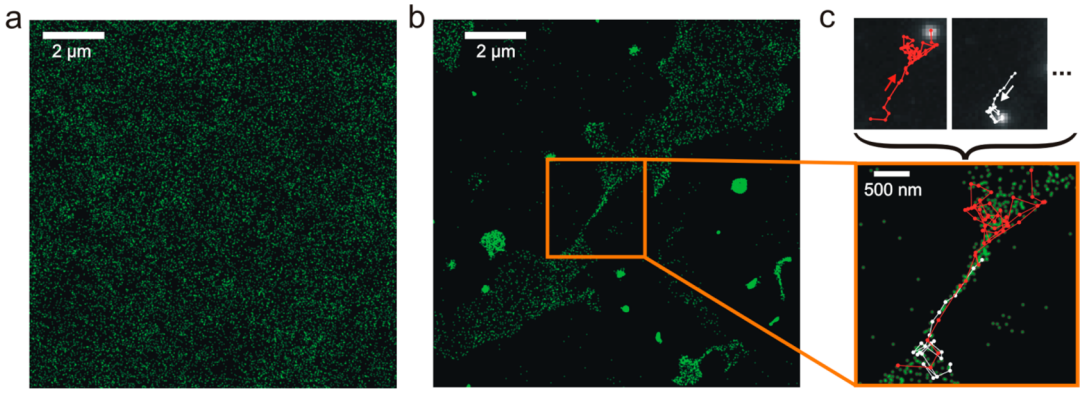

Figure 3. Super-resolution reconstructions derived from the patterns of diffusion of DNA barges with continuous (a) or discontinuous (b,c) deposition of lipids on a glass slide (*A*:*C*:*P* = 1:1:0; DOPC-only membrane in PBS buffer). (c) Magnified view of a narrow isthmus traced out by multiple diffusing DNA barges; two representative trajectories of DNA barges are shown in red and white.

anomalous diffusion function MSD = $4D\tau^{\alpha}$, we calculated an average diffusion coefficient $\langle D \rangle = 0.71\ \mu m^2/s$ (Figure 2e), which is similar to the value of $1.39\ \mu m^2/s$ reported recently for membrane-bound DNA origami rods as determined by fluorescence correlation spectroscopy[17] and within the range of $0.05-2.6\ \mu m^2/s$ reported for lipid-linked peripheral proteins in similar model membranes.[27,28] Values of the time exponent α, derived from MSD fitting, cluster around a mean value of 1.001, indicating that barges undergo normal Brownian diffusion in the supported lipid bilayer. Interestingly, two or more DNA barges are often observed to occupy the same diffraction-limited region and appear to undergo correlated motion for periods of 0.2−0.5 s (Figure S7, Supporting Information), suggesting that they may transiently form complexes within the bilayer *via* nonspecific blunt-end stacking, electrostatic, or cholesterol−cholesterol interactions. Consistent with this observation, the distribution of barge intensities exhibits a single majority peak (comprising 84% of all particles) with only a small peak of approximately twice the majority peak intensity (Figure S8, Supporting Information), indicating a small steady-state population of such putative complexes.

Next, we investigated an application of DNA barges as super-resolution probes of membrane structure. In contrast to small lipophilic dyes such as Nile Red, which can map the structure of lipid membranes by transient association from bulk solution,[29] DNA barges remain stably bound over time. They hence trace out only *contiguous regions* of fluid bilayer, as would a membrane-associated protein, making them sensitive to local discontinuities. When a microscope slide was uniformly coated with a lipid bilayer, an image reconstructed using the coordinates from tracks of diffusing DNA barges showed an essentially uniform density of localizations after an imaging period of ∼1 min (Figure 3a). By contrast, when the lipids were deposited on the surface at a ∼5-fold lower concentration, forming discontinuous patches, the corralled diffusion of DNA barges painted a super-resolution image of islands, isthmuses, and objects consistent with small spherical vesicles (Figures 3b,c and S9, Supporting Information). Since each DNA nanostructure carries dozens of copies of fluorophore, individual barges are visible through the ocular lens of our microscope under low illumination ($10-30\ W/cm^2$), making them particularly useful when imaging for long time periods, when aiming for the highest possible localization accuracy, or when using less sensitive microscopes. Notably, the DNA barges utilized here have a large footprint (∼60 × 90 nm) relative to our localization accuracy (13.8 nm as determined from immobile barges on an uncoated glass surface), so that the outmost boundaries of lipid patches may be undersampled in super-resolution reconstructions, just as they would be by a large, diffusing, membrane-associated protein complex. However, their highly configurable size and shape could permit probing of membrane structure on different length scales.

To test the capacity of DNA barges as membrane-anchored agents for delivery of molecular payloads, as well as to verify the solvent accessibility of the barges, we designed experiments to transfer bound Cargo strands to and from bulk solution. After embedding DNA barges labeled with a 1:1:2 mixture of *A*:*C*:*P* in a DOPC/DOPE-mPEG bilayer, we added an ssDNA "fuel" (*F*) strand that can specifically remove *C* from the barge *via* its toehold,[30] resulting in a rapid decrease in fluorescence (Figure 4a). When an excess of *C* was then flushed into the sample chamber for Cargo reloading, the fluorescence of the barges quickly increased to nearly the original level. Thus, the Cargo-bearing side of the DNA barges facing the membrane is capable of exchanging nearly all of its Cargo with solution, acting as a source and sink for a large reservoir of Cargo molecules in repeated exchanges. By contrast, when a 1:3:0 mixture of *A*:*C*:*P* was used for the assembly of the barges and the same *C* removal and reloading experiment was performed, then both the decrease and recovery of fluorescence are less complete (Figure S10, Supporting Information). Noticing that the rate of

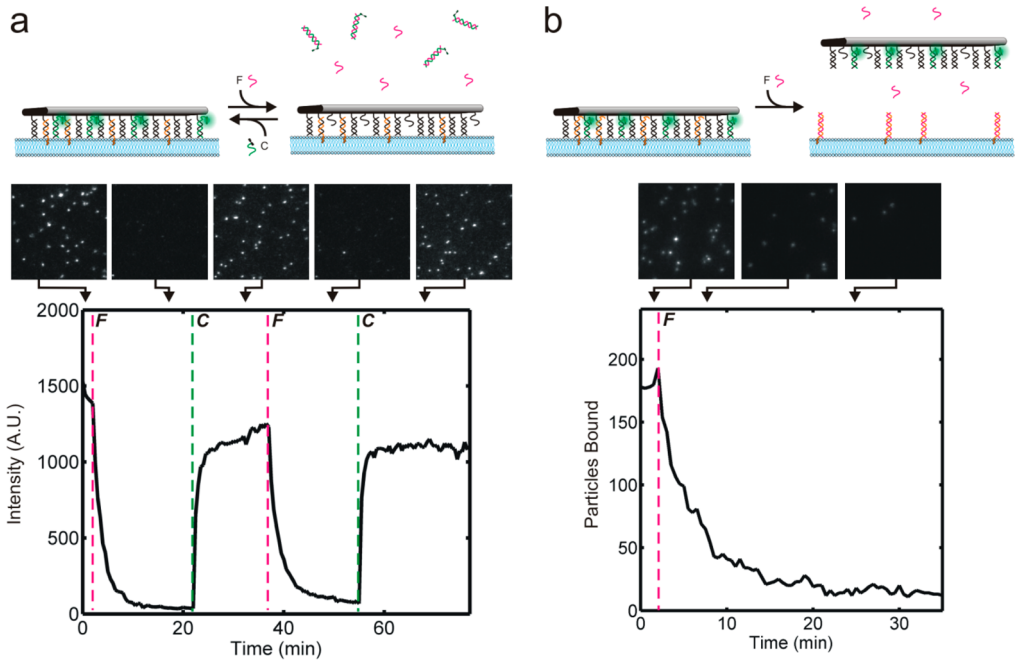

Figure 4. Programmable exchange of cargo and lift-off of barges from DOPC/DOPE-mPEG bilayers. (a) A Fuel strand (*F*) binds to the fluorescent Cargo (*C*) *via* an 8-nucleotide toehold and displaces it from the DNA barge, causing a decrease in the intensity of all barges within a field of view. Introducing fresh Cargo results in nearly complete reloading of barges assembled with a 1:1:2 mixture of *A*:*C*:*P*. (b) Lift-off from a supported lipid bilayer is achieved by moving the 8-nt toehold sequence to the cholesterol-labeled anchor. Upon addition of *F*, the anchors are displaced from the barges, and the majority of barges dissociate from the bilayer.

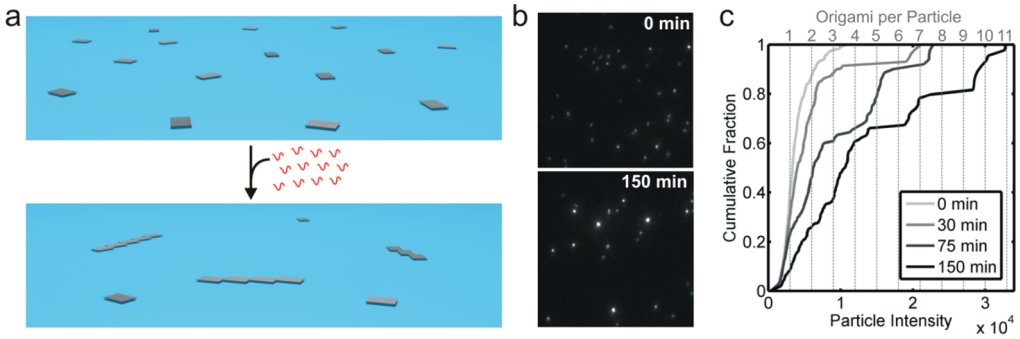

Figure 5. Triggered oligomerization of membrane-associated DNA barges. (a) Diagonal oligomerization of DNA origami tiles is induced by adding 12 short linker ssDNA strands (red). (b) Representative region showing the number and intensity of fluorescent particles within a supported lipid bilayer before and 150 min after linker strand addition. (c) Intensity-weighted cumulative histogram of particle intensities 0−150 min after adding the linker strands. The estimated number of origami tiles per particle (top axis and dashed gray lines) is based on multiples of the mean intensity (~3000) of the majority population at time 0 as determined by Gaussian fitting of the intensity distribution (Figure S8, Supporting Information). The concentration of fluorescence signal into brighter puncta over time is consistent with the formation of oligomers containing 2−10 origami each.

diffusion of the 1:3:0 *A*:*C*:*P* DNA barges irreversibly slows down upon *C* removal (Figure S10, Supporting Information; 83% of barges have $D < 0.01\ \mu m^2/s$), we hypothesize that removing the majority of *C* strands from a barge, which leaves behind their ssDNA capture probes, results in tighter association with the bilayer, slowing diffusion and blocking accessibility to the Cargo loading sequence. This hypothesis is consistent with the more complete loading and somewhat more rapid diffusion after Cargo exchange of the 1:1:2 *A*:*C*:*P* barges (Figures 4a and S10, Supporting Information; 59% of barges have $D > 0.01\ \mu m^2/s$) since the presence of the toehold-free and thus nonexchangeable spacer *P* reduces the fraction of capture probes converted to ssDNA upon *C* removal. We posit that the surface a DNA nanostructure presents to a lipid bilayer, *i.e.*, single-stranded or double-stranded, affects its diffusive properties as well as its ability to interact with components from solution.

We next tested whether the same strand displacement strategy could be used to induce detachment of the DNA barges from a lipid bilayer by removing the cholesterol anchor *A* from the 1:1:2 *A*:*C*:*P* DNA barges. For this experiment, we moved the toehold sequence from *C* to *A* (resulting in the strands *C*′ and *A*′), thus

allowing the fuel strand *F* to disrupt instead the interaction between *A*′ and the origami. As expected based on the cholesterol dependence of membrane embedding (Figure 2b), the removal of *A*′ resulted in a marked decline in the number of barges bound to the bilayer (Figure 4b). Thus, the association of DNA origami with a lipid bilayer can also be controlled using oligonucleotide commands.

Finally, we examined the potential to rationally engineer interactions between DNA origami embedded within the lipid bilayer. Using a previously published strategy to link rectangular origami into linear filaments,[31] we injected a mixture of 12 specific ssDNA linker strands into a sample chamber with a supported lipid bilayer populated with DNA barges (Figure 5a) and measured the distribution of particle intensities over time. After addition of the linker strands, the observed fluorescence over time became concentrated into a smaller number of more intense puncta, consistent with the stepwise oligomerization of ~80% of all observed barges into short filaments containing 2−10 origami barges each at the end of the 150 min observation window (Figure 5b,c). Interestingly, the barges diffuse more slowly once oligomerized ($\langle D \rangle$ = 0.010 $\mu m^2/s$), and the largest (*i.e.*, brightest) complexes become essentially stationary on the time scale of observation. The molecular origin of this effect is not clear, but it suggests that there may be a practical upper limit to the size of membrane-embedded DNA barge complexes. Importantly, neither the slowing of diffusion nor the concentration of intensity into puncta was observed in the absence of linker strands (Figure S4, Supporting Information), demonstrating that this is a response to a specific oligonucleotide command.

CONCLUSIONS

In summary, we have shown that DNA−cholesterol barges associate with and diffuse laterally within synthetic supported lipid bilayers in a manner that depends on a lipophilic label (cholesterol), membrane composition, buffer/salt conditions, and the type of interface presented to the bilayer by the DNA tile. Our results suggest that interactions between lipid-modified DNA nanostructures and bilayers can be rationally modulated by altering the number and distribution of chemical groups (single- *versus* double-stranded DNA, lipids) presented to the bilayer. DNA barges can be used as fluorescent super-resolution probes of membranous structures, and may provide a novel, highly configurable approach to the characterization of biological membranes and cytoskeletal organization within living cells. Notably, the length scale of tens of nanometers that characterizes DNA origami structures is well-matched to the 30−230 nm size of diffusion corrals observed in biological membranes.[32] We have also shown that DNA barges can undergo programmable interactions with external components in solution or within the membrane, opening up possibilities for the rational design of sophisticated membrane-bound chemical systems such as artificial signal transduction cascades. It may also be possible to achieve tighter orientational control over some chemical processes by using diffusible membrane-bound nanostructures to direct interactions between reactive components. Cells fully exploit biological membranes for many important and complex processes, and it is likely that this approach will prove equally useful in synthetic systems.

MATERIALS AND METHODS

Preparation of DNA−Cholesterol Barges. All oligonucleotides used for the assembly of nanostructures were purchased from Integrated DNA Technologies, Inc. (www.idtdna.com). *P* was purified by denaturing polyacrylamide gel electrophoresis (PAGE; 10% (w/v) 19:1 acrylamide:bis-acrylamide in 1 × TBE buffer: 89 mM Tris base, 89 mM boric acid, 2 mM EDTA, pH 8.0); *C*, *C*′, *A*, and *A*′ oligonucleotides were HPLC-purified by the manufacturer. *F* and the linker oligonucleotides were purified by standard desalting and used without further purification.

Rectangular origami tiles[19] were prepared by mixing M13mp18 viral DNA scaffold (Affymetrix) with 202 staple strands at a 1:3 molar ratio in 1 × TA-Mg^{2+} buffer (40 mM Tris base, 20 mM acetic acid, 12.5 mM $Mg(CH_3COO)_2$). The final concentration of M13mp18 in each assembly reaction was 10 nM. 187 of the 202 staple strands were extended at their 5′-end with the probe sequence (5′-CCT CTC ACC CAC CAT TCA TC) and purified by denaturing polyacrylamide gel electrophoresis. For origami tiles assembled here, staples 1−12 and 205−216 of the original design were omitted to prevent intertile base stacking interactions that result in undesirable aggregation.[19] The mixture was heated to 90 °C and cooled to 4 °C over 12 h using an automated PCR thermocycler (Mastercycler Pro, Eppendorf). Origami tile preparations were stored at 4 °C and used within 2 months.

DNA barges were prepared by incubating assembled origami tiles at room temperature for 5−10 min with a ~10-fold total molar excess (relative to binding sites) of the appropriate oligos *C* (5′-/5Cy3/TCA ATA ATG ATG AAT GGT GGG TGA GAG G), *A* (5′-GAT GAA TGG TGG GTG AGA GG/3CholTEG/), and/or *P* (5′-GAT GAA TGG TGG GTG AGA GG). In the sequences, the underlined segment represents the toehold for strand displacement by *F* (5′-CCT CTC ACC CAC CAT TCA TCA TTA TTG A). In the case of lift-off experiments, the variants *C*′ (5′-/5Cy3/TT GAT GAA TGG TGG GTG AGA GG) and *A*′ (5′-TCA ATA ATG ATG AAT GGT GGG TGA GAG G/3CholTEG/) were used in place of *C* and *A*, respectively, to enable displacement of the cholesterol-labeled anchor strand. The total concentration of *C*/*C*′, *A*/*A*′, and *P* oligos was 4 μM during assembly, which is sufficient for binding to reach completion in less than 5 min (compare to binding kinetics of only 200 nM *C* in Figure 4a). Once prepared, the barges were either diluted to 50−200 pM in TA-Mg^{2+} buffer for single-molecule measurements or combined with loading buffer (6X loading buffer: TA-Mg^{2+} with 50% glycerol) and loaded directly onto agarose gels for electrophoresis.

Characterization of DNA Barge Assembly and Aggregation. A 10 nM solution of DNA origami tiles was spiked with 5 μM of a nonbinding Cy5-labeled ssDNA strand (5′-/5Cy5/CCG CGT TCC ATC CTT TCT TAC CT) to serve as a gel loading control. The DNA origami tiles were combined with varying ratios of *C* and either *A* or *P* (total concentration: 4 μM) in TA-Mg^{2+} for 10 min at room temperature. The samples were separated by electrophoresis

on a 0.5% agarose gel containing TAE-Mg^{2+} (40 mM Tris base, 20 mM acetic acid, 12.5 mM $Mg(CH_3COO)_2$, 2 mM EDTA, pH 7.8) in a water bath at room temperature (22 °C; gel temperature increased to ~27 °C). Since many commercial loading buffers contain EDTA and lack magnesium, a 6× loading buffer containing 50% glycerol in TA-Mg^{2+} was prepared and used in order to maintain the integrity of DNA origami tiles during loading. Gels were scanned on a Typhoon 9410 Variable Mode Imager (GE Healthcare Life Sciences) using excitation and emission filter settings for Cy3 detection, and the total fluorescence intensity of each lane (excluding the fast-migrating band resulting from free *C*) was quantified using ImageQuant, normalizing each lane with respect to its Cy5 loading control. Results from three replicates were averaged and then normalized to the fluorescence intensity of the 100% *C* lane.

We assume that the Cy3 fluorescence intensity I_{Cy3} observed for each DNA barge preparation depends on the relative kinetics of binding of the two competing strands (either *C* and *A* or *C* and *P*) according to $I_{Cy3} = \alpha * k_C f_C/(k_C f_C + k_2 f_2)$, where k_C and f_C are the pseudo-first-order binding rate constant and mole fraction of *C*, respectively, k_2 and f_2 are the rate constant and mole fraction of either *A* or *P*, and α is a proportionality constant. Since $f_C + f_2 = 1$, we can rearrange this relationship to

$$I_{Cy3} = \alpha\left[1 - \frac{\left(\frac{k_2}{k_C}\right) f_2}{\left(\frac{k_2}{k_C} - 1\right) f_2 + 1}\right] \quad (1)$$

Eq 1 was fit to the plots of normalized Cy3 intensity as a function of f_2 (Figure S1b,c, Supporting Information) to estimate k_A/k_C and k_P/k_C, the relative rates of oligonucleotide binding to the DNA origami tile.

Characterization of Cholesterol-Labeled Anchor Strand Aggregation. Denaturing PAGE characterization of *A* and *P* was performed using 10% acrylamide with 8.3 M urea in 1× TBE buffer (89 mM Tris base, 89 mM boric acid, 2 mM EDTA, pH 8.0), with 50 pmol DNA per well. Nondenaturing PAGE of *A*, *C*, and *P* was performed using 10% acrylamide in 1 × TAE-Mg^{2+} at 10 °C, with 500 pmol DNA per well. The O'RangeRuler 10 bp DNA Ladder (Thermo) was used as a size marker in the native gel, and the 10 bp DNA Ladder (Life Technologies) was used in the denaturing gel. The gels were stained with ethidium bromide (native gel) or SYBR gold (denaturing gel) and scanned with a Biorad Gel Doc XR+ system. The size distribution of micelles formed by *A* in water was measured using a Zetasizer Nano ZS (Malvern) and processed with Zetasizer software (ver. 6.32).

Preparation of Lipid Bilayers. The lipids 1,2-dioleoyl-*sn*-glycero-3-phosphocholine (DOPC, # 850375P) and 2-dioleoyl-*sn*-glycero-3-phosphoethanolamine-*N*-[methoxy(poly(ethylene glycol))-550] (DOPE-mPEG, # 880530C) were purchased from Avanti Polar Lipids, suspended in chloroform (Fisher, BP1145−1) to concentrations of 20 and 10 mg/mL, respectively, and stored at −20 °C.

Our method of preparing lipid bilayers is based on previously published work.[33,34] To prepare lipid vesicle suspensions, clean glass vials (Fisherbrand, 15 × 85 mm) were rinsed with water and ethanol and dried in an oven at 130 °C for 30−60 min before cooling to room temperature. Chloroform suspensions of either DOPC or a 12.5:1 mixture of DOPC:DOPE-mPEG were added to the glass vials and dried under nitrogen while vortexing to remove chloroform. The resulting lipid cake was further dried under a vacuum overnight to remove any trace chloroform, and then resuspended to 10 mg/mL in lipid buffer (10 mM Tris-HCl, pH 8.0, 100 mM NaCl) over a period of 1−2 h. The suspension was vortexed vigorously, then extruded 11 times through a 0.2-μm polycarbonate filter (Whatman Nuclepore), and finally extruded 11 times through a 0.1-μm polycarbonate filter. For super-resolution imaging experiments, the 10 mg/mL DOPC mixture was instead extruded only 3 times through a 0.20 μm nylon syringe filter (Fisherbrand). The resulting lipid vesicle suspensions were stored at 4 °C for 1−2 weeks.

To prepare supported lipid bilayers, vesicle suspensions were diluted in lipid buffer to ~0.8 mg/mL (~0.16 mg/mL in the case of patchy lipid bilayers, Figures 3b,c and S9, Supporting Information). A 1 mL portion of the suspension was injected into the fluidic channel of a quartz microscope slide fitted with plastic tubing as described[35] over three additions, with a 5−10 min waiting period after each addition. Each slide was gently washed with 1 mL of lipid buffer to remove excess lipid, and the bilayers were allowed to heal for 30 min prior to injecting DNA barge samples.

Fluorescence Microscopy. Imaging was performed on a home-built prism-type TIRF microscope[35−38] based on an Olympus IX-71 frame and using a 1.2 NA 60× water immersion objective (UPlanApo, Olympus). Excitation was provided by a 532 nm laser (CL532−050-L, CrystaLaser), which was attenuated using neutral density filters and focused to produce a power of ~30 W/cm^2 in the sample plane. The image from the microscope was relayed using two dichroic mirrors (cutoff wavelength 610 nm, Chroma) and passed through an emission filter (HQ580/60, Chroma) before being projected onto an iCCD camera (iPentamax:HQ, Princeton Instruments). Images were acquired at 10 Hz. For Cargo loading/unloading, lift-off, barge oligomerization, and barge binding kinetics measurements, frame acquisitions were interrupted by dark periods (see below) to minimize photobleaching. All imaging was performed in the presence of an oxygen scavenger system (OSS, 25 nM protocatechuate dioxygenase +2.5 mM protocatechuic acid +1 mM Trolox).[39]

Kinetics of DNA Barge Binding to Lipid Bilayers. Suspensions of DNA barges assembled with 1:1:2 ("+ cholesterol") or 1:0:3 ("− cholesterol") mixtures of *A*:*C*:*P* oligonucleotides were diluted to 20 pM in TA-Mg^{2+} + OSS. While monitoring fluorescence by TIRF microscopy, a 200-μL volume was gently injected into the fluidic chamber of a microscope slide containing a DOPC or DOPC/DOPE-mPEG supported lipid bilayer. The number of fluorescent particles visible in a single 100 × 50 μM field of view was calculated for each frame of the movie using custom MATLAB code that identified DNA barges as local intensity maxima within each frame after suppressing noise below an intensity threshold of 25 counts.

Single-Particle Tracking and Mean Squared Displacement Analysis. Suspensions of DNA barges assembled with a 1:1:2 mixture of *A*:*C*:*P* were diluted to 50 pM in TA-Mg^{2+}. A 100-μL volume was injected into the fluidic chamber of a quartz microscope slide containing a DOPC/DOPE-mPEG supported lipid bilayer. After a 2 min incubation, excess unbound barges were flushed out with 200 μL of TA-Mg^{2+} + OSS. Diffusion of barges was monitored by TIRF microscopy for 60 s in each of 6 different fields of view. Particle diffusion was analyzed using the MOSAIC[40] plug-in for ImageJ.[41]

Time-averaged mean squared displacement (MSD)[42] analysis was performed using custom MATLAB code and the EzyFit toolbox (Frédéric Moisy). Only trajectories of barges remaining within the field of view and well-separated from other barges for at least 5 s were analyzed. The maximum time lag (τ) used in the MSD analysis was restricted to 12 frames to avoid noise from poorly determined MSD values in short trajectories. For the trajectory shown in Figure 2c,d, a longer trajectory was analyzed with time lags up to 25 frames (2.5 s).

Fluorescence Recovery after Photobleaching. Supported lipid bilayers containing either DOPC or a 12.5:1 mixture of DOPC:DOPE-mPEG were prepared on glass slides as described above. For FRAP measurements, 0.1% (w/w) 1,2-dioleoyl-*sn*-glycero-3-phosphoethanolamine-*N*-(lissamine rhodamine B sulfonyl) (Avanti Polar Lipids) was included in the lipid mixtures. Membrane fluorescence under excitation at 532 nm was determined by averaging rhodamine emission intensity over a ~50 × 25 μm^2 region in the center of the field of view. A shuttered illumination scheme (0.1 s exposure, 59.9 s dark period) was used to minimize photobleaching. After verifying the stability of fluorescence over a period of ~5 min, the entire field of view was bleached under constant illumination for 2 min, and the recovery of fluorescence monitored for ~40 min under shuttered illlumination.

Super-Resolution Imaging. Suspensions of DNA barges assembled with a 1:1:0 mixture of *A*:*C*:*P* oligonucleotides were diluted to 200 pM in phosphate-buffered saline (PBS, pH 7.4, Life Technologies). A 100-μL volume was injected into the fluidic chamber of a quartz microscope slide containing a DOPC supported lipid bilayer. After a 2 min incubation, excess unbound barges were flushed out with 200 μL of PBS + OSS.

Diffusion of barges was monitored by TIRF microscopy for 500 s (patchy bilayer, Figure 3b) or 1500 s (contiguous bilayer, Figure 3a).

The super-resolution reconstructions shown in Figure 3 were generated as follows. First, the QuickPALM[43] plug-in for ImageJ was used to localize all barges within each frame of the movie. Then, a reconstruction was generated by plotting the coordinates from the QuickPALM output as symmetric 2-D Gaussian functions with standard deviations of 13.8 nm (corresponding to the mean localization accuracy as determined from the standard deviations of localization measurements on 71 DNA barges immobilized on a glass slide). The DNA barge trajectories shown in Figure 3c were generated by 2-D Gaussian fitting using custom MATLAB code and subsequently plotted over the super-resolution reconstruction.

Cargo Exchange. Suspensions of DNA barges assembled with a 1:1:2 or 1:3:0 mixture of *A*:*C*:*P* were diluted to 200 pM in TA-Mg^{2+}. A 100-μL volume was injected into the fluidic chamber of a quartz microscope slide containing a DOPC/DOPE-mPEG supported lipid bilayer. After a 2 min incubation, excess unbound barges were flushed out with 200 μL of TA-Mg^{2+} + OSS. Barge diffusion in a single field of view was characterized by particle tracking and subsequent MSD analysis according to the procedure outlined above.

While monitoring barge fluorescence using TIRF microscopy and a shuttered illumination scheme consisting of 0.1-s acquisition periods separated by 29.9-s dark periods, 200 μL of 200 nM Fuel (*F*, 5′-CCT CTC ACC CAC CAT TCA TCA TTA TTG A) in TA-Mg^{2+} + OSS was injected into the slide's fluidic chamber to unload the Cargo by toehold-mediated strand displacement. After the average fluorescence signal in the field of view became constant over several consecutive frames, 200 μL of 20 nM Cargo (*C*) in TA-Mg^{2+} + OSS was injected. This cycle was repeated once. After two consecutive Cargo exchange cycles, the diffusion of DNA barges was again characterized in a single field of view.

The time-dependent intensity of DNA barges was determined as follows. DNA barges were identified as local maxima within each frame after suppressing noise below an intensity threshold of 25 counts. The intensity of each DNA barge was calculated by first subtracting a background image generated by morphological opening of the original image with a disk-shaped structural element 15 pixels in diameter ("imopen" function in MATLAB), then summing the intensity values within a 5 × 5-pixel square region centered on each barge. The total intensity of all barges visible within each frame (~200) was summed and then divided by the number of barges in the first frame of observation to generate the time traces shown in Figures 4a and S10d (Supporting Information).

Lift-off from Supported Lipid Bilayers. Suspensions of DNA barges assembled with a 1:1:2 mixture of *A*′:*C*′:*P* were diluted to 50 pM in TA-Mg^{2+}. A 100-μL volume was injected into the fluidic chamber of a quartz microscope slide containing a DOPC/DOPE-mPEG supported lipid bilayer. After a 2 min incubation, excess unbound barges were flushed out with 200 μL of TA-Mg^{2+} + OSS.

While monitoring barge fluorescence using TIRF microscopy and a shuttered illumination scheme consisting of 0.1-s acquisition periods separated by 29.9-s dark periods, 200 μL of 500 nM Fuel (*F*) in TA-Mg^{2+} + OSS was injected into the slide's fluidic chamber to displace the *A*′ anchor from the DNA barges by toehold-mediated strand displacement. The number of barges bound in each movie frame was determined by the same spot-finding algorithm used in the Cargo exchange experiments.

Oligomerization of Membrane-Associated Barges. Suspensions of DNA barges assembled with a 1:1:2 mixture of *A*:*C*:*P* were diluted to 500 pM in TA-Mg^{2+}. A 100-μL volume was injected into the fluidic chamber of a quartz microscope slide containing a DOPC/DOPE-mPEG supported lipid bilayer. After a 2 min incubation, excess unbound barges were flushed out with 200 μL of TA-Mg^{2+} + OSS.

While monitoring barge fluorescence using TIRF microscopy and a shuttered illumination scheme consisting of 0.1-s acquisition periods separated by 14.9-s dark periods, 200 μL of a mixture of 12 linker strands[31] (sequences shown in Table S1, Supporting Information), each at a concentration of 100 nM in TA-Mg^{2+} + OSS, was injected into the slide's fluidic chamber to induce oligomerization of membrane-bound barges. The intensity distribution of all barges observed in each movie frame was determined by the same algorithms used in the Cargo exchange experiments. Cumulative intensity histograms for time points of 0, 30, 75, and 150 min after addition of the linker strands were calculated from particle intensity values in five consecutive frames (constituting a 1 min time window). Cumulative histograms were intensity-weighted: *i.e.*, the *y*-axis represents the fraction of total fluorescence *intensity* (not the fraction of particles) that fall within particles of a given intensity value and thus serves as a proxy for the fraction of all barges concentrated into oligomeric particles.

Conflict of Interest: The authors declare no competing financial interest.

Acknowledgment. This work was funded in part by the Department of Defense MURI Award W911NF-12-1-0420. The authors acknowledge the assistance of X. Su in some single-molecule experiments.

Supporting Information Available: Movie of cholesterol-dependent binding of DNA barges to DOPC/DOPE-mPEG bilayers; linker strand sequences used in barge oligomerization; agarose gels and atomic force microscopy of barge assembly and aggregation; PAGE and DLS of cholesterol-labeled anchor strand aggregation; kinetics of barge binding to DOPC/DOPE-mPEG bilayer; fluorescence recovery after photobleaching measurements of supported lipid bilayers; control for aggregation and lift-off experiments; lateral diffusion of a DNA barge nonspecifically bound to a lipid bilayer; time-lapse images of DNA barges bound to supported lipid bilayers containing DOPC or to a bare glass surface; example of apparent transient interaction between two DNA barges within a lipid bilayer; intensity histograms of DNA barges; apparent diffusion of a DNA barge about an isolated lipid vesicle; slowing of diffusion and incomplete reloading upon displacement of Cargo from DNA barges. This material is available free of charge *via* the Internet at http://pubs.acs.org.

REFERENCES AND NOTES

1. Schlessinger, J. The Mechanism and Role of Hormone-Induced Clustering of Membrane Receptors. *Trends Biochem. Sci.* **1980**, *5*, 210–214.
2. Axelrod, D. Lateral Motion of Membrane Proteins and Biological Function. *J. Membr. Biol.* **1983**, *75*, 1–10.
3. McCloskey, M. A.; Poo, M. M. Rates of Membrane-Associated Reactions: Reduction of Dimensionality Revisited. *J. Cell Biol.* **1986**, *102*, 88–96.
4. McCloskey, M. A.; Poo, M. M. Contact-Induced Redistribution of Specific Membrane Components: Local Accumulation and Development of Adhesion. *J. Cell Biol.* **1986**, *102*, 2185–2196.
5. Stryer, L. Cyclic GMP Cascade of Vision. *Annu. Rev. Neurosci.* **1986**, *9*, 87–119.
6. Hackenbrock, C. R.; Chazotte, B.; Gupte, S. S. The Random Collision Model and a Critical Assessment of Diffusion and Collision in Mitochondrial Electron Transport. *J. Bioenerg. Biomembr.* **1986**, *18*, 331–368.
7. Liebman, P. A.; Parker, K. R.; Dratz, E. A. The Molecular Mechanism of Visual Excitation and Its Relation to the Structure and Composition of the Rod Outer Segment. *Annu. Rev. Physiol.* **1987**, *49*, 765–791.
8. Metzger, H.; Kinet, J. P. How Antibodies Work: Focus on Fc Receptors. *FASEB J.* **1988**, *2*, 3–11.
9. Lenaz, G. Role of Mobility of Redox Components in the Inner Mitochondrial Membrane. *J. Membr. Biol.* **1988**, *104*, 193–209.
10. Lavergne, J.; Joliot, P. Restricted Diffusion in Photosynthetic Membranes. *Trends Biochem. Sci.* **1991**, *16*, 129–134.
11. Heldin, C.-H. Dimerization of Cell Surface Receptors in Signal Transduction. *Cell* **1995**, *80*, 213–223.
12. Holowka, D.; Baird, B. Antigen-Mediated IGE Receptor Aggregation and Signaling: A Window on Cell Surface

Structure and Dynamics. *Annu. Rev. Biophys. Biomol. Struct.* **1996**, *25*, 79–112.
13. Lamb, T. D. Gain and Kinetics of Activation in the G-Protein Cascade of Phototransduction. *Proc. Natl. Acad. Sci. U. S. A.* **1996**, *93*, 566–570.
14. Langecker, M.; Arnaut, V.; Martin, T. G.; List, J.; Renner, S.; Mayer, M.; Dietz, H.; Simmel, F. C. Synthetic Lipid Membrane Channels Formed by Designed DNA Nanostructures. *Science* **2012**, *338*, 932–936.
15. Burns, J. R.; Stulz, E.; Howorka, S. Self-Assembled DNA Nanopores That Span Lipid Bilayers. *Nano Lett.* **2013**, *13*, 2351–2356.
16. Burns, J. R.; Göpfrich, K.; Wood, J. W.; Thacker, V. V.; Stulz, E.; Keyser, U. F.; Howorka, S. Lipid-Bilayer-Spanning DNA Nanopores with a Bifunctional Porphyrin Anchor. *Angew. Chem., Int. Ed.* **2013**, *52*, 12069–12072.
17. Czogalla, A.; Petrov, E. P.; Kauert, D. J.; Uzunova, V.; Zhang, Y.; Seidel, R.; Schwille, P. Switchable Domain Partitioning and Diffusion of DNA Origami Rods on Membranes. *Faraday Discuss.* **2013**, *161*, 31.
18. Sarveswaran, K.; Hu, W.; Huber, P. W.; Bernstein, G. H.; Lieberman, M. Deposition of DNA Rafts on Cationic SAMs on Silicon [100]. *Langmuir* **2006**, *22*, 11279–11283.
19. Rothemund, P. W. K. Folding DNA to Create Nanoscale Shapes and Patterns. *Nature* **2006**, *440*, 297–302.
20. Amunts, A.; Drory, O.; Nelson, N. The Structure of a Plant Photosystem I Supercomplex at 3.4 Å Resolution. *Nature* **2007**, *447*, 58–63.
21. Umena, Y.; Kawakami, K.; Shen, J.-R.; Kamiya, N. Crystal Structure of Oxygen-Evolving Photosystem II at a Resolution of 1.9 A. *Nature* **2011**, *473*, 55–60.
22. Mullineaux, C. W.; Tobin, M. J.; Jones, G. R. Mobility of Photosynthetic Complexes in Thylakoid Membranes. *Nature* **1997**, *390*, 421–424.
23. Johnson-Buck, A.; Nangreave, J.; Jiang, S.; Yan, H.; Walter, N. G. Multifactorial Modulation of Binding and Dissociation Kinetics on Two-Dimensional DNA Nanostructures. *Nano Lett.* **2013**, *13*, 2754–2759.
24. Ainalem, M.-L.; Kristen, N.; Edler, K. J.; Höök, F.; Sparr, E.; Nylander, T. DNA Binding to Zwitterionic Model Membranes. *Langmuir* **2010**, *26*, 4965–4976.
25. Sofia, S. J.; Premnath, V.; Merrill, E. W. Poly(ethylene Oxide) Grafted to Silicon Surfaces: Grafting Density and Protein Adsorption. *Macromolecules* **1998**, *31*, 5059–5070.
26. Roy, R.; Hohng, S.; Ha, T. A Practical Guide to Single-Molecule FRET. *Nat. Methods* **2008**, *5*, 507–516.
27. Fein, M.; Unkeless, J.; Chuang, F. Y.; Sassaroli, M.; da Costa, R.; Väänänen, H.; Eisinger, J. Lateral Mobility of Lipid Analogues and GPI-Anchored Proteins in Supported Bilayers Determined by Fluorescent Bead Tracking. *J. Membr. Biol.* **1993**, *135*, 83–92.
28. Ziemba, B. P.; Falke, J. J. Lateral Diffusion of Peripheral Membrane Proteins on Supported Lipid Bilayers Is Controlled by the Additive Frictional Drags of (1) Bound Lipids and (2) Protein Domains Penetrating into the Bilayer Hydrocarbon Core. *Chem. Phys. Lipids* **2013**, *172*−*173*, 67–77.
29. Sharonov, A.; Hochstrasser, R. M. Wide-Field Subdiffraction Imaging by Accumulated Binding of Diffusing Probes. *Proc. Natl. Acad. Sci. U. S. A.* **2006**, *103*, 18911–18916.
30. Zhang, D. Y.; Winfree, E. Control of DNA Strand Displacement Kinetics Using Toehold Exchange. *J. Am. Chem. Soc.* **2009**, *131*, 17303–17314.
31. Li, Z.; Liu, M.; Wang, L.; Nangreave, J.; Yan, H.; Liu, Y. Molecular Behavior of DNA Origami in Higher-Order Self-Assembly. *J. Am. Chem. Soc.* **2010**, *132*, 13545–13552.
32. Murase, K.; Fujiwara, T.; Umemura, Y.; Suzuki, K.; Iino, R.; Yamashita, H.; Saito, M.; Murakoshi, H.; Ritchie, K.; Kusumi, A. Ultrafine Membrane Compartments for Molecular Diffusion as Revealed by Single Molecule Techniques. *Biophys. J.* **2004**, *86*, 4075–4093.
33. Granéli, A.; Yeykal, C. C.; Prasad, T. K.; Greene, E. C. Organized Arrays of Individual DNA Molecules Tethered to Supported Lipid Bilayers. *Langmuir* **2006**, *22*, 292–299.
34. Finkelstein, I. J.; Greene, E. C. Supported Lipid Bilayers and DNA Curtains for High-Throughput Single-Molecule Studies. In *DNA Recombination*; Tsubouchi, H., Ed.; Methods in Molecular Biology; Humana Press: New York, 2011; pp 447−461.
35. Michelotti, N.; de Silva, C.; Johnson-Buck, A. E.; Manzo, A. J.; Walter, N. G. A Bird's Eye View: Tracking Slow Nanometer-Scale Movements of Single Molecular Nano-Assemblies. *Methods Enzymol.* **2010**, *475*, 121–148.
36. Walter, N. G.; Huang, C.-Y.; Manzo, A. J.; Sobhy, M. A. Do-It-Yourself Guide: How to Use the Modern Single-Molecule Toolkit. *Nat. Methods* **2008**, *5*, 475–489.
37. Pereira, M. J. B.; Nikolova, E. N.; Hiley, S. L.; Jaikaran, D.; Collins, R. A.; Walter, N. G. Single VS Ribozyme Molecules Reveal Dynamic and Hierarchical Folding Toward Catalysis. *J. Mol. Biol.* **2008**, *382*, 496–509.
38. Ditzler, M. A.; Rueda, D.; Mo, J.; Håkansson, K.; Walter, N. G. A Rugged Free Energy Landscape Separates Multiple Functional RNA Folds Throughout Denaturation. *Nucleic Acids Res.* **2008**, *36*, 7088–7099.
39. Aitken, C. E.; Marshall, R. A.; Puglisi, J. D. An Oxygen Scavenging System for Improvement of Dye Stability in Single-Molecule Fluorescence Experiments. *Biophys. J.* **2008**, *94*, 1826–1835.
40. Sbalzarini, I. F.; Koumoutsakos, P. Feature Point Tracking and Trajectory Analysis for Video Imaging in Cell Biology. *J. Struct. Biol.* **2005**, *151*, 182–195.
41. Abramoff, M. D.; Magalhães, P. J.; Ram, S. J. Image Processing with ImageJ. *Biophotonics Int.* **2004**, *11*, 36–42.
42. Andreanov, A.; Grebenkov, D. S. Time-Averaged MSD of Brownian Motion. *J. Stat. Mech.: Theory Exp.* **2012**, P07001.
43. Henriques, R.; Lelek, M.; Fornasiero, E. F.; Valtorta, F.; Zimmer, C.; Mhlanga, M. M. QuickPALM: 3D Real-Time Photoactivation Nanoscopy Image Processing in ImageJ. *Nat. Methods* **2010**, *7*, 339–340.